LIMNOLOGY AND OCEANOGRAPHY
Letters

ASLO
Open Access

Limnology and Oceanography Letters 2022

doi: 10.1002/lol2.10260

LETTER

Interpreting consequences of inadequate sampling of oceanic motions

Chuanyin Wang,[1] *Zhiyu Liu*,[1]* *Hongyang Lin*[1,2]*

[1]State Key Laboratory of Marine Environmental Science, and Department of Physical Oceanography, College of Ocean and Earth Sciences, Xiamen University, Xiamen, China; [2]Southern Marine Science and Engineering Guangdong Laboratory (Zhuhai), Zhuhai, China

Scientific Significance Statement

Recent studies revealed that the estimated energy distribution of internal gravity waves (IGWs) in the frequency-wavenumber space is heavily dependent on the data-sampling rate. Undersampling (or aliasing) results in peculiar spectral features and impedes sound physical interpretations. Properly interpreting these features remains challenging for the community. In this study, we assess spectral manifestation of undersampled IGWs under varying spatiotemporal sampling rates to illustrate that (1) spectral features of hourly undersampled rather than daily-undersampled IGWs can be predicted in principle and (2) spatial subsampling tends to discard spectral energies directly rather than fold them to the low-wavenumber end (aliasing), compared with temporal subsampling. This study has important implications for the interpretation of ocean model results and oceanographic measurements by the upcoming next-generation altimetry missions.

Abstract

Inadequate sampling of oceanic motions, which commonly occurs for both oceanic measurements and simulations, can cause peculiar spectral features and potentially leads to misinterpretations. Here, we combine an extremely high-frequency moored velocity record and a high-resolution numerical simulation with the basic signal-processing theory to quantitatively explore how varying sampling rates affect the ability to represent oceanic motions, especially internal gravity waves (IGWs). The moored measurements and simulations demonstrate that hourly sampling is sufficient to capture horizontal internal tidal velocities, but inadequate to faithfully characterize the vertical velocity for nearly all frequencies. The daily-sampled model simulation shows a complicated frequency-wavenumber spectral pattern of IGWs. Due to contrasting periodicities in time and space, temporal subsampling tends to retain the total variance of original IGWs, while spatial subsampling directly induces spectral energy loss. This study sheds light on data applications of the upcoming satellite altimetry missions.

*Correspondence: zyliu@xmu.edu.cn and hylin@xmu.edu.cn

Associate editor: Stephen Monismith

Author Contribution Statement: The corresponding authors ZL and HL conceived the idea and designed the study. The first author CW carried out the specific analysis. All authors contribute to interpretation of the results and writing of the final manuscript.

Data Availability Statement: The LLC4320 simulation output is available at https://data.nas.nasa.gov/ecco/data.php?dir=/eccodata/llc_4320. The moored current observations used in this study can be downloaded from https://doi.org/10.17605/OSF.IO/E6WXB.

Additional Supporting Information may be found in the online version of this article.

When a periodic signal is discretely sampled, the components of the signal with frequencies higher than half the sampling frequency (i.e., Nyquist frequency) will be indistinguishable from lower-frequency components. Those unresolved high-frequency signals are termed aliased and this phenomenon is denoted aliasing. Aliasing is a well-known problem in digital signal processing. In geoscience, it is particularly relevant to analysis of both observations (especially moored observations of temporal variations) and numerical modeling results. On the one hand, the aliased frequencies are predictable, which can be utilized to recover the real signals. An established example is that physical oceanographers exploit the periodic nature of internal tides (ITs) to extract coherent ITs from satellite altimetric data subject to aliasing (Ray and Mitchum 1996; Kantha and Tierney 1997; Ray and Cartwright 2001; Carrère et al. 2004; Dushaw 2015; Ray and Zaron 2016; Zhao et al. 2016; Zhao 2017; Zaron 2019). This represents an ingenious application of temporal aliasing to quantitatively characterize processes that are not adequately resolved by the actual sampling rate. On the other hand, aliasing more generally causes distortions of original signals and hence poses difficulties in accurately revealing resolved processes and can even lead to misinterpretations.

Recently, global tide-resolving and submesoscale-admitting simulations, which explicitly resolve multiscale oceanic motions including barotropic tides, large-scale circulations, mesoscale motions, internal gravity waves (IGWs), etc., have become available. Limited by storage space, these model results are often stored as snapshots with a time interval much larger than the time-marching step of the simulation. In this case, spectral quantification of resolved variabilities is hindered by an intriguing pattern of aliasing in the estimated frequency-wavenumber spectra (Savage et al. 2017; Qiu et al. 2019). For example, in the analysis of the frequency-wavenumber spectra of the hourly snapshots of sea surface height (SSH) for different regions of the world's ocean, Savage et al. (2017) and Arbic et al. (2018) noticed that the spectral energy around dispersion relation curves of IGWs significantly folded back after reaching the Nyquist period (i.e., 2 h), inducing overlap with other oceanic motions, such as submesoscale processes. They explained that hourly snapshots of SSH could not resolve the high-frequency IGWs and therefore subhourly IGWs (i.e., IGWs with frequencies higher than hourly) underwent temporal aliasing with the spectral energy folding back to lower frequencies. The vertical velocity was similarly aliased (Qiu et al. 2019), which is an even more severe issue due to the fact that the vertical IGW velocity has more spatiotemporally fine-scale features.

However, the two-dimensional aliasing pattern in the frequency-wavenumber spectra remains to be unambiguously quantified and its influence on resolved processes clearly elucidated. This is particularly relevant to the application of next-generation altimetric data that are inevitably subject to temporal and/or spatial aliasing. To this end, we first subsample the hourly output of a high-resolution numerical simulation, both in space and time. Then, the dependence of frequency-wavenumber spectra of SSH and surface vertical velocity on the sampling strategy is examined for two oceanic regions with contrasting IGW energy levels. We also perform complementary explorations based on moored measurements to examine the aliasing effect of subhourly variabilities, which can not be resolved in hourly model outputs.

Data and methods

In this study, we use the output of a global tide-resolving and submesoscale-admitting simulation, which explicitly resolves multiscale oceanic motions. It is a global 1/48° configuration (i.e., LLC4320) of the Massachusetts Institute of Technology general circulation model (MITgcm) and has been extensively employed. Forced by the full luni-solar tidal potential and 6-hourly atmospheric fields, the LLC4320 simulation outputs hourly snapshots for 14 months from September 2011 to November 2012. For more detailed descriptions of the configuration, readers are referred to Arbic et al. (2018) and http://wwwcvs.mitgcm.org/viewvc/MITgcm/MITgcm_contrib/llc_hires/. Previous studies show that multiscale motions are well reproduced in this simulation, including large-scale circulations (Wang et al. 2018), barotropic tides (Lin et al. 2020), mesoscale variabilities (Qiu et al. 2018), IGWs (Savage et al. 2017), and submesoscale features (Lin et al. 2020). Therefore, the LLC4320 simulation is well suited for this study.

For comparison, we selected model outputs for the central South China Sea (SCS; Fig. 1a) with strong ITs but weak

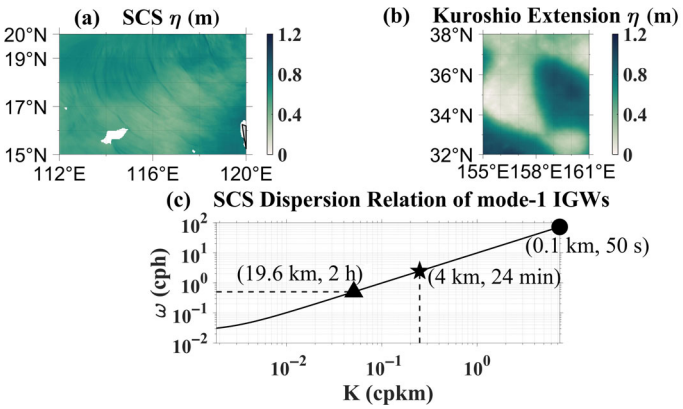

Fig. 1. SSH snapshots for the (**a**) SCS, (**b**) Kuroshio Extension, and (**c**) the dispersion relation of mode-1 IGWs in the SCS. The dispersion relation curve (solid black) at (116°E, 17.5°N) is calculated from the output of the MITgcm LLC4320 simulation. The Nyquist period associated with the time interval of the model output, the Nyquist wavelength associated with the horizontal grid spacing of the simulation, and the Nyquist period associated with the time-marching step of the simulation are indicated by the triangle, star, and bullet, respectively. The corresponding wavelength and period are labeled.

mesoscale variabilities and for the Kuroshio Extension (Fig. 1b) with weak ITs but energetic mesoscale activities. ITs are IGWs with tidal periods (12.42 h for M_2, 12.0 h for S_2, 23.93 h for K_1, and 25.84 h for O_1). To mimic the temporal (~ 1 d) and spatial resolution (~ 10 km) of the upcoming next-generation altimetry missions (Chen et al. 2019), such as Guanlan and Surface Water and Ocean Topography (SWOT), the model outputs (hourly, ~ 2 km) were subsampled on a 1-d (i.e., 24 h) and 10-km basis.

Because inertia-gravity waves are the main superinertial motions, their spectral estimates are prone to aliasing when the sampling frequency is inadequate. Inertia-gravity waves in the ocean consist of a barotropic mode, mainly in the form of barotropic tides, and an infinite number of baroclinic modes, namely IGWs. Since barotropic tides are in general long waves with wavelengths of $O(10^3$ km) in the open ocean, they are not spatially aliased and can be readily extracted through low-pass spatial filtering. Therefore, we mainly focus on aliasing of IGWs.

Evidently, for a simulation with a horizontal grid spacing of ~ 2 km and a time-marching step of 25 s, the grid spacing is the limiting factor as seen in Fig. 1c, which gives the dispersion relation curve of the fastest, mode-1 IGWs in the SCS, together with the Nyquist period/wavelength corresponding to the time-marching step, outputting time interval and horizontal grid spacing of the LLC4320 simulation. Thus, the fastest IGWs possibly resolved by the simulation have a period of 24 min with a wavelength of ~ 4 km. With the model simulation stored hourly, IGWs with a period greater than 24 min and less than the Nyquist period of 2 h are inevitably aliased. Similarly, if the hourly outputs are daily subsampled, most of the IGWs are subject to temporal aliasing, since IGWs typically have periods less than 2 d (many IGWs are tides and tidal periods are roughly 12 and 24 h, which are both less than 2 d). If the daily outputs are further subsampled onto horizontal grids with a spacing of 10 km, IGWs with wavelengths between ~ 4 km and 20 km will be aliased. Other oceanic processes are similarly subject to temporal and/or spatial aliasing.

Note that aliasing occurs according to a well-defined mathematical principle (Bendat and Piersol 2011; Cushman-Roisin and Beckers 2011; Wunsch 2015). Assume that ω_N is the Nyquist frequency, then $[-\omega_N,\omega_N]$ is the frequency ranges that a time series can resolve. Any frequency ω outside the range $[-\omega_N,\omega_N]$ will be aliased into $\omega_a = \omega - 2n\omega_N$, where n is an integer such that ω_a falls within $[-\omega_N,\omega_N]$. Therefore, given the original frequency, we can readily predict the exact aliased frequency and thus the aliased dispersion relation of IGWs. This allows us to clearly quantify aliasing. Spatial aliasing takes place exactly in the same manner.

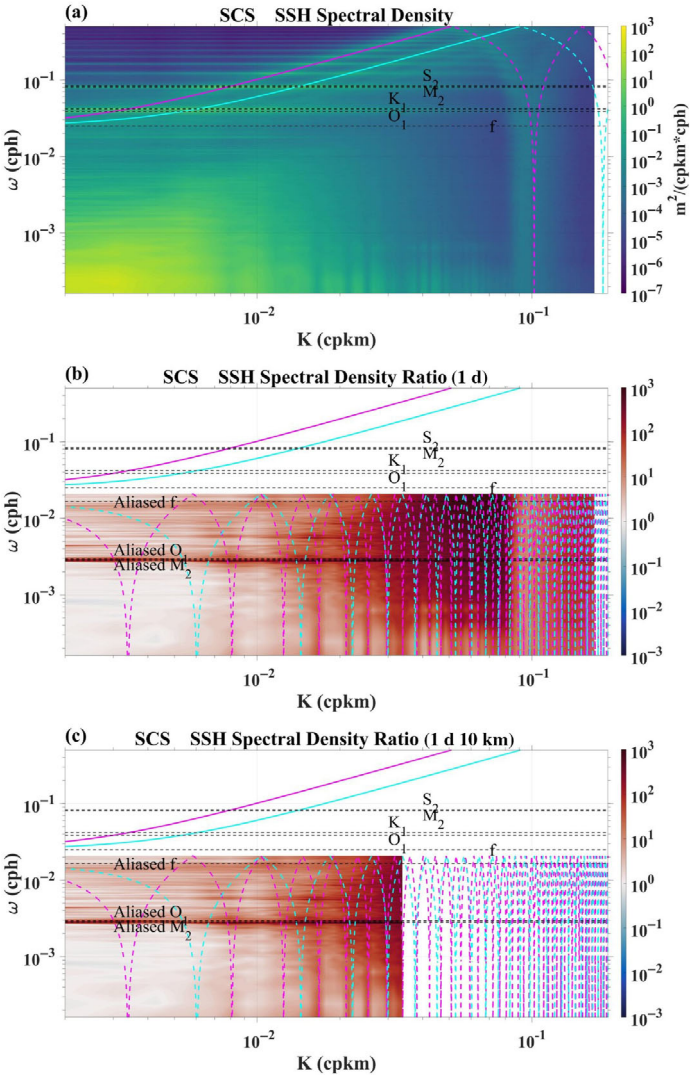

Fig. 2. The frequency-wavenumber spectral density of the original SSH and spectral density ratios of the subsampled SSH in the SCS. The panels display (**a**) the spectral density calculated from the original hourly model output, (**b**) the spectral density ratio of the daily-subsampled SSH to the original hourly model output, and (**c**) the spectral density ratio of the subsampled SSH on a 1-d and 10-km basis to the original hourly model output. The solid/dashed magenta (cyan) curves denote the original/temporally aliased mode-1 (mode-2) dispersion relation of IGWs. The dashed black lines show the original and temporally aliased diurnal (K_1, O_1), semidiurnal (M_2, S_2) tidal frequencies, and inertial frequency in the middle of the study region. For simplicity, we do not consider aliasing due to spatial subsampling in Fig. 2c when plotting the dispersion relation curves.

Results

Figures 2a and 3a show the frequency-wavenumber spectra of SSH in the SCS and Kuroshio Extension, respectively. It is clear that mesoscale motions contribute most of the subinertial variance of hourly SSH both in the SCS and Kuroshio Extension. The superinertial energy is dominated by mode-1 and mode-2 IGWs following the resolved dispersion relation curves. Especially, ITs manifest themselves as major semidiurnal and diurnal constituents as well as their superharmonics.

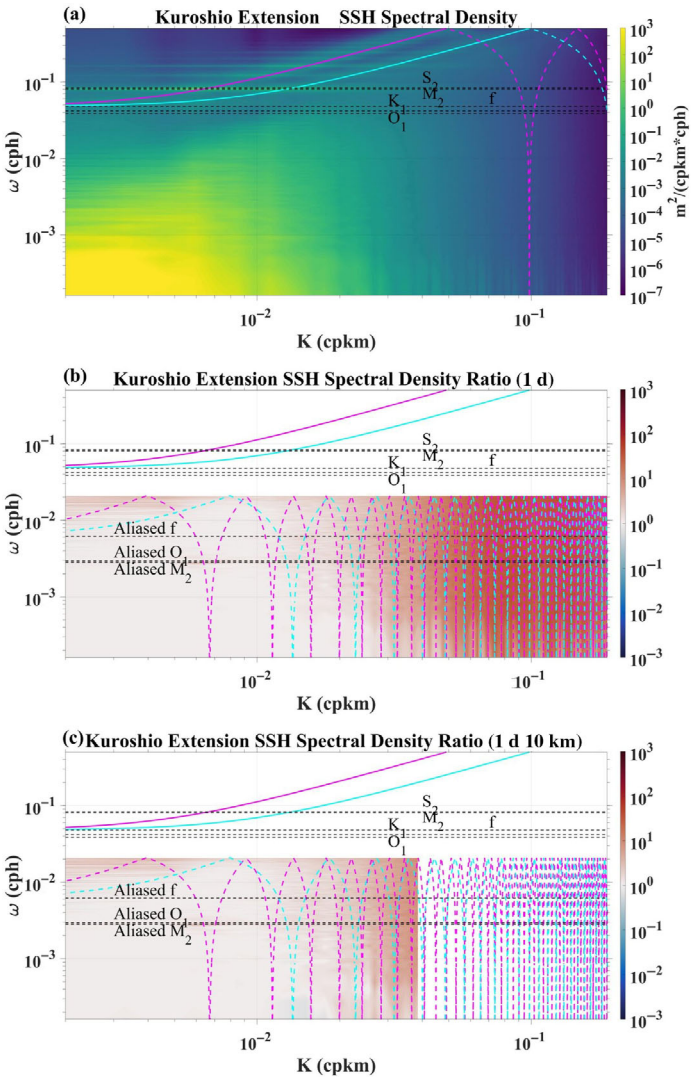

Fig. 3. Same as Fig. 2 but for the Kuroshio Extension.

Note that no freely propagating diurnal ITs are present around the Kuroshio Extension since it is located poleward of the diurnal critical latitude (where the local inertial period equals the diurnal period). Strikingly, due to the strong ITs in the SCS, the aliased mode-1 IGWs are also clearly identifiable in the spectra, as indicated by the large spectral energies exactly along the theoretically predicted dashed magenta curve in Fig. 2a. This quantitatively and unambiguously supports previous interpretation of temporal aliasing of IGWs due to inadequate model outputting rate (Savage et al. 2017; Arbic et al. 2018; Qiu et al. 2019). In contrast, the Kuroshio Extension is characterized by weak ITs so that there is no identifiable aliasing in the spectra.

When the hourly data are daily subsampled, all of the dispersion relation curves of IGWs are aliased to be the intricate dashed ones in Figs. 2b and 3b, which show the spectral density ratio of the daily-subsampled SSH to the original hourly SSH in the SCS and Kuroshio Extension, respectively. The energy folding greatly increases the spectral density at low frequencies, overshadowing the original variabilities, particularly in the SCS. This is also clearly demonstrated in Fig. 4 (more precisely Fig. 4a,c), which shows wavenumber and frequency spectra obtained through integration of the frequency-wavenumber spectra in Figs. 2 and 3. Consequently, the aliased spectral density does not seem to clearly follow the aliased dispersion relation curves. However, the energetic M_2 constituent manages to stand out and peaks at the predicted value (Figs. 2b, 3b, 4a,c), although it is more noticeable in the SCS because of the strong ITs and less clear in the Kuroshio Extension due to the intense mesoscale motions. The aliased O_1 spectral energy is also significant in Figs. 2b and 4a. The manifestation of main aliased tidal frequencies is precisely the basis of the abovementioned extraction of coherent ITs from altimetric SSH. The aliased S_2 peak vanishes completely since its intrinsic frequency is precisely an integer multiple of the 1-d sampling frequency and is thus aliased to the zero frequency (mean). The same rationale applies to the invisible aliased K_1 peak. When it comes to the corresponding wavenumber spectra, mild energy loss is seen at the low-wavenumber range, but is still insignificant in the SCS (Fig. 4b). In the Kuroshio Extension, wavenumber spectra are almost unchanged (Fig. 4d), indicating little energy loss through the daily subsampling despite the vanishing peaks of K_1 and S_2. This striking feature indicates that due to its strong temporal periodicity, the total variance of IGWs, even with temporally insufficient sampling, can be almost completely retained.

In addition to temporal aliasing, high-wavenumber motions are aliased into the low-wavenumber band arising from spatial subsampling as seen in Figs. 2c and 3c, the spectral density ratio of the subsampled SSH on a 1-d and 10-km basis to the original hourly SSH in the SCS and Kuroshio Extension, respectively. In striking contrast to temporal aliasing, such wavenumber-domain aliasing is nearly negligible (clearer in Fig. 4b,d) and the high-wavenumber energy seems to be directly discarded rather than folded back. This seems understandable since IGWs generally appear more periodic in time than in space which was previously shown by modeling results (Ponte and Klein 2015) and indicated by observations (Vic et al. 2021). Correspondingly, the frequency spectral energy associated with both temporal and spatial subsampling in the SCS is reduced at the high-frequency end (Fig. 4a), indicating a striking loss of total spectral energy.

As discussed above, variabilities of SSH are mostly characterized by superinertial IGWs and subinertial mesoscale motions. In contrast, the vertical velocities are dominated by IGW variabilities and possibly submesoscale motions (Klein and Lapeyre 2009). Furthermore, the vertical velocities of IGWs have higher contributions from spatially finer scales as mentioned in the introductory section. Hence, the associated

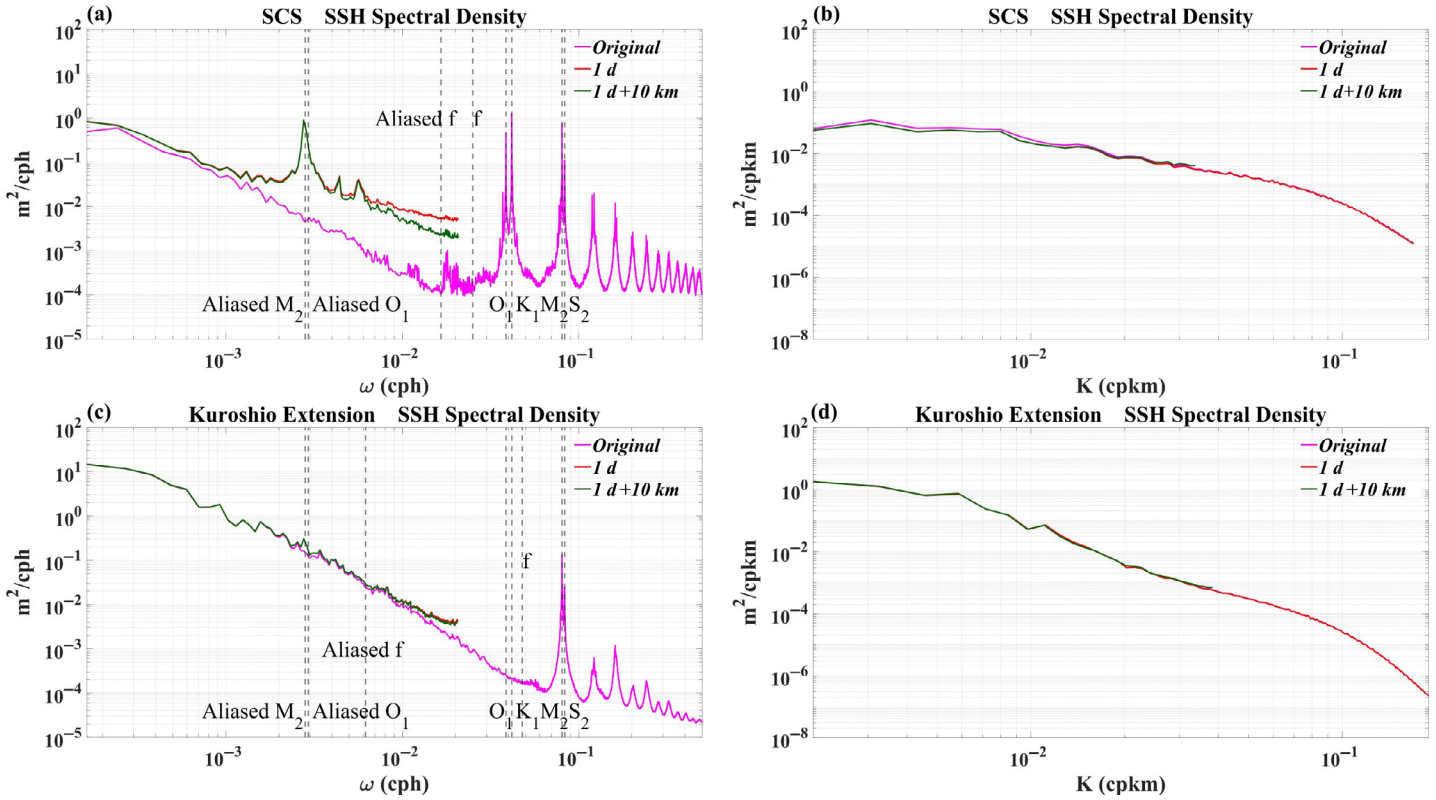

Fig. 4. The wavenumber and frequency spectral density of SSH in the SCS (**a**, **b**) and the Kuroshio Extension (**c**, **d**). The spectral density without data subsampling is denoted by the magenta line. The spectral density with data daily subsampled is shown by the red line. The spectral density with data subsampled on a 1-d and 10-km basis is represented by the green line. The vertical dashed black lines indicate the original and aliased diurnal (K_1, O_1), semidiurnal (M_2, S_2) tidal frequencies and inertial frequency in the middle of the study region.

aliasing is anticipated to be more noticeable in vertical velocities than in SSH. Therefore, we applied the similar analysis to the surface vertical velocity (Figs. S1–S3 in the Supporting Information). As expected, most spectral energy of the surface vertical velocity is contributed by mode-1 and mode-2 IGWs (Figs. S1a, S2a). The hourly aliased mode-1 IGWs exhibit nearly as strong variance as that of resolved IGWs, closely following the aliased dispersion relation curve all the way to the lowest frequency and folding back (the magenta dashed curve in Figs. S1a, S2a). Temporal subsampling significantly changes the spectral distribution of the originally weak low-frequency energy (Figs. S1b, S2b), leaving aliased IGWs to peak around M_2 (Fig. S3a,c). Unlike SSH, the associated reduction of wavenumber spectral energies due to the daily subsampling is non-negligible in the SCS (Fig. S3b). Further spatial subsampling moderately increases the wavenumber spectral energy, particularly for the SCS (Figs. S1c, S2c, S3b,d), but noticeably reduces the frequency spectral energy for both regions (Fig. S3a,c). Consequently, a marked amount of energy is lost during the spatiotemporal subsampling of the vertical velocity, especially for the SCS. Otherwise, the spectra of the vertical velocity and SSH share similarities.

Summary and discussion

Recent studies indicate an interesting aliasing pattern in the frequency-wavenumber domain (Savage et al. 2017; Qiu et al. 2019). To better understand this aliasing effect, we subsample a high-resolution model simulation (with a grid spacing of ~ 2 km and hourly output) at coarser temporal and spatial resolutions according to the designed resolutions of future altimetry missions. We then perform the spectral analysis of SSH and surface vertical velocity from two dynamically contrasting regions (i.e., the SCS and Kuroshio Extension). It is shown that to characterize IGWs without aliasing, the outputting frequency and spatial resolution should be coupled according to the dispersion relation of mode-1 IGWs. The aliasing effect is explored in detail by comparing the aliased spectral patterns of SSH and surface vertical velocity against the original patterns and the aliased dispersion relation. Generally, the intricate, aliased patterns of subsampled data render it difficult to identify the full IGW continuum. In oceanic regions with strong ITs such as the SCS, a substantial spectral energy loss would arise from combined temporal and spatial subsampling of SSH, while a marked amount of spectral energy of the surface vertical velocity

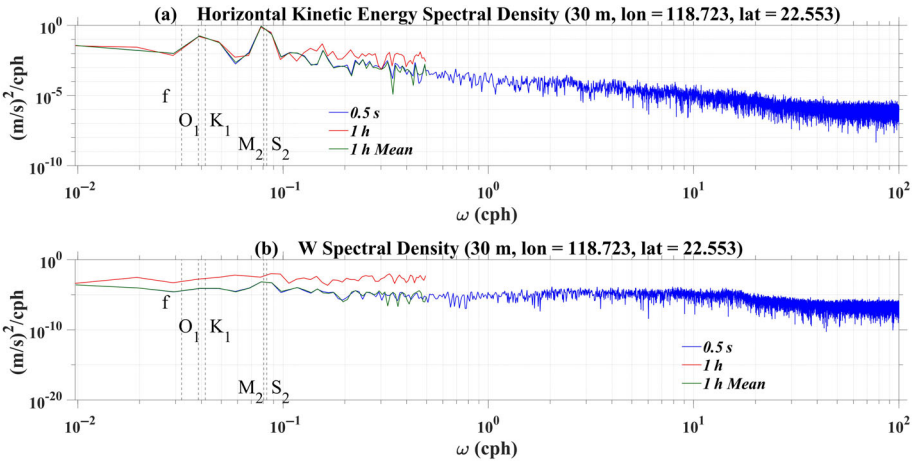

Fig. 5. The spectral density of the horizontal kinetic energy (**a**) and vertical velocity (**b**) at 30 m from a mooring in the Taiwan Strait. The spectral density calculated directly from measured data is shown by the blue line. The spectral density with data hourly subsampled is shown by the red line. The spectral density with data hourly averaged is represented by the green line. The vertical dashed black lines indicate the diurnal (K_1, O_1), semidiurnal (M_2, S_2) tidal frequencies and inertial frequency.

would be lost whenever temporal or spatial subsampling is performed. In regions with weak ITs such as the Kuroshio Extension, the corresponding spectral energy loss of SSH is negligible, while that of the surface vertical velocity is non-negligible only when the temporal and spatial subsamplings are conducted simultaneously.

As pointed out by Savage et al. (2017), Arbic et al. (2018), and Qiu et al. (2019), quantitatively shown in Figs. 2a and S1a, and explained in the Results section, IGWs show significant subhourly variabilities and thus hourly snapshots experience aliasing. To evaluate the aliasing effect of subhourly processes, moored velocity measurements (Wang et al. 2021) with a sampling time interval of 0.5 s in the Taiwan Strait are used. Similar to the treatment of LLC4320 data, we subsample the moored velocity measurements with an hourly interval and compare spectral properties of the original and subsampled velocity measurements. For the horizontal velocity (Fig. 5a), the hourly subsampling manages to capture diurnal and semidiurnal tides, but fails to characterize higher-frequency IGWs in terms of both spectral magnitude and variation. For the vertical velocity (Fig. 5b), the hourly subsampling heavily contaminates the observed spectra at nearly all frequencies. It indicates that hourly snapshots of vertical velocity cannot accurately characterize multiscale oceanic motions. To efficiently alleviate the aliasing problem, temporal averaging over a certain interval, instead of snapshot subsampling, is recommended (green lines in Fig. 5a,b). This should be taken as a basic principle for sampling both observational and model output data. The present study has thus shed light on the understanding and application of space-borne (e.g., Guanlan and SWOT) and *in situ* oceanographic measurements.

References

Arbic, B. K., and others. 2018. A primer on global internal tide and internal gravity wave continuum modeling in HYCOM and MITgcm, p. 307–392. *In New Frontiers in operational oceanography*. GODAE OceanView. doi:10.17125/gov2018.ch13

Bendat, J. S., and A. G. Piersol. 2011, *Random data: Analysis and measurement procedures*, v. **729**. John Wiley & Sons.

Carrère, L., C. Le Provost, and F. Lyard. 2004. On the statistical stability of the M_2 barotropic and baroclinic tidal characteristics from along-track TOPEX/Poseidon satellite altimetry analysis. J. Geophys. Res. Oceans **109**: 1–13. doi:10.1029/2003jc001873

Chen, G., and others. 2019. Concept design of the "Guanlan" science mission: China's novel contribution to space oceanography. Front. Mar. Sci. **6**: 1–14. doi:10.3389/fmars.2019.00194

Cushman-Roisin, B., and J. M. Beckers. 2011, *Introduction to geophysical fluid dynamics: Physical and numerical aspects*. p. 789. Academic Press.

Dushaw, B. D. 2015. An empirical model for mode-1 internal tides derived from satellite altimetry: Computing accurate tidal predictions at arbitrary points over the world oceans. http://www.apl.washington.edu/project/%0Aprojects/tm_1-15/pdfs/tm_1_15.pdf

Kantha, L. H., and C. C. Tierney. 1997. Global baroclinic tides. Prog. Oceanogr. **40**: 163–178. doi:10.1016/S0079-6611(97)00028-1

Klein, P., and G. Lapeyre. 2009. The oceanic vertical pump induced by mesoscale and submesoscale turbulence. Ann. Rev. Mar. Sci. **1**: 351–375. doi:10.1146/annurev.marine.010908.163704

Lin, H., Z. Liu, J. Hu, D. Menemenlis, and Y. Huang. 2020. Characterizing meso- to submesoscale features in the South China Sea. Prog. Oceanogr. **188**: 102420. doi:10.1016/j.pocean.2020.102420

Ponte, A. L., and P. Klein. 2015. Incoherent signature of internal tides on sea level in idealized numerical simulations. Geophys. Res. Lett. **42**: 1520–1526. doi:10.1002/2014GL062583

Qiu, B., S. Chen, P. Klein, H. Torres, J. Wang, L. L. Fu, and D. Menemenlis. 2019. Reconstructing upper ocean vertical velocity field from sea surface height in the presence of unbalanced motion. J. Phys. Oceanogr. **49**: 55–79. doi:10.1175/JPO-D-19-0172.1

Qiu, B., S. Chen, P. Klein, J. Wang, H. Torres, L.-L. Fu, and D. Menemenlis. 2018. Seasonality in transition scale from balanced to unbalanced motions in the world ocean. J. Phys. Oceanogr. **48**: 591–605. doi:10.1175/JPO-D-17-0169.1

Ray, R. D., and E. D. Zaron. 2016. M_2 internal tides and their observed wavenumber spectra from satellite altimetry. J. Phys. Oceanogr. **46**: 3–22. doi:10.1175/JPO-D-15-0065.1

Ray, R. D., and D. E. Cartwright. 2001. Estimates of internal tide energy fluxes from Topex/Poseidon altimetry: Central North Pacific. Geophys. Res. Lett. **28**: 1259–1262. doi:10.1029/2000GL012447

Ray, R. D., and G. T. Mitchum. 1996. Surface manifestation of internal tides generated near Hawaii. Geophys. Res. Lett. **23**: 2101–2104. doi:10.1029/96GL02050

Savage, A. C., and others. 2017. Spectral decomposition of internal gravity wave sea surface height in global models. J. Geophys. Res. Oceans **122**: 7803–7821. doi:10.1002/2017JC013009

Vic, C., B. Ferron, V. Thierry, H. Mercier, and P. Lherminier. 2021. Tidal and near-inertial internal waves over the Reykjanes Ridge. J. Phys. Oceanogr. **51**: 419–437. doi:10.1175/JPO-D-20-0097.1

Wang, C., Liu, Z., Cao, Z., Hu, Z., Zhang, F. 2021. Spectra of moored velocity measurements in the Taiwan Strait. doi:10.17605/OSF.IO/E6WXB

Wang, J., and others. 2018. An observing system simulation experiment for the calibration and validation of the Surface Water Ocean Topography sea surface height measurement using in situ platforms. J. Atmos. Oceanic Tech. **35**: 281–297. doi:10.1175/JTECH-D-17-0076.1

Wunsch, C. 2015, *Modern Observational Physical Oceanography: Understanding the Global Ocean*. Princeton Univ. Press.

Zaron, E. D. 2019. Baroclinic tidal sea level from exact-repeat mission altimetry. J. Phys. Oceanogr. **49**: 193–210. doi:10.1175/JPO-D-18-0127.1

Zhao, Z. 2017. The global mode-1 S_2 internal tide. J. Geophys. Res. Oceans **122**: 8794–8812. doi:10.1002/2017JC013112

Zhao, Z., M. H. Alford, J. B. Girton, L. Rainville, and H. L. Simmons. 2016. Global observations of open-ocean mode-1 M_2 internal tides. J. Phys. Oceanogr. **46**: 1657–1684. doi:10.1175/JPO-D-15-0105.1

Acknowledgments

This work was supported by the National Natural Science Foundation of China (NSFC; 91858201, 42076013, 41730533, 41890801, and 41721005), and the Natural Science Foundation of Fujian Province of China (2021J02005 and 2019J05009). Robert Scott is thanked for sharing his code to calculate frequency-wavenumber spectra (http://stockage.univ-brest.fr/~scott/scripts.html). We thank the crew of the *RV* Yanping II for their assistance in data collection during the open research cruise NORC2020-04 supported by NSFC Shiptime Sharing Project (41949904); thanks go to Fangtao Zhang in particular for organizing such an incredible cruise. Zhiyong Cao and Zhendong Hu are thanked for quality-controlling moored current observations and helpful discussions. Constructive comments from the editors and two anonymous referees are greatly appreciated. Robin Robertson kindly helped improve the presentation of this paper. This work is a part of C. Wang's PhD research at the Dynamical Oceanography Group (DyOG) of Xiamen University. C. Wang would like to thank all other members of DyOG for their kind efforts to create an environment that is scientifically stimulating and socially comfortable.

Submitted 28 December 2021
Revised 29 April 2022
Accepted 02 May 2022